A R C H I V E S O F M E T A L L U R G Y A N D M A T E R I A L S
Volume 59 2014 Issue 2
DOI: 10.2478/amm-2014-0097

S. WROŃSKI*, K. WIERZBANOWSKI*, M. WROŃSKI*, B. BACROIX**

THREE DIMENSIONAL ANALYSIS OF ASYMMETRIC ROLLING WITH FLAT AND INCLINED ENTRY

TRÓJWYMIAROWA ANALIZA WALCOWANIA ASYMETRYCZNEGO Z PŁASKIM ORAZ UKOŚNYM WEJŚCIEM MATERIAŁU

The results of three-dimensional simulation of asymmetric rolling, using Finite Elements Method, are presented. The example case of low carbon steel is considered. The rolling asymmetry, considered in the present work, results from different angular velocities of two identical working rolls. The effects of asymmetry on stress and strain distributions, material bending and variations of normal force and torque exerted by rolls are calculated and discussed. A special emphasis is done on the influence of inclined entry of a rolled material, which can appear in sequential rolling. Such the entry can partly compensate the material bending during. The results of the present simulations show that optimum parameters can be found in order to minimize the effect of sheet curvature and to reduce the applied torque and normal rolling force.

The predicted internal stress distributions were applied next in the crystallographic deformation model; the predicted textures of symmetric and asymmetric rolling are in good agreement with experimental results.

Keywords: asymmetric rolling, inclined entry, deformation model, Finite Element Method, texture, residual stress, internal stress

W pracy przedstawiono wyniki trójwymiarowej symulacji walcowania asymetrycznego, używając Metody Elementów Skończonych. Rozważono walcowanie stali niskowęglowej. Asymetria walcowania, rozważana w niniejszej pracy, wynika z różnych prędkości kątowych dwóch identycznych walców. Przedyskutowano wpływ asymetrii walcowania na rozkłady naprężeń i odkształceń, wygięcie materiału oraz modyfikację siły i momentu obrotowego wywieranego przez walce. Szczególną uwagę zwrócono na możliwość ukośnego wprowadzania materiału, które może występować w walcowaniu sekwencyjnym. Takie wprowadzanie materiału może częściowo zrekompensować jego wygięcie. Wyniki niniejszych obliczeń wskazują, że można znaleźć optymalne parametry w celu redukcji do minimum wygięcia blach i zmniejszenia siły i momentu sił wywieranych przez walce.

Wyliczone rozkłady naprężeń wewnętrznych zastosowano następnie w krystalograficznym modelu deformacji; przewidywane tekstury walcowania symetrycznego i asymetrycznego pozostają w dobrej zgodności z danymi doświadczalnymi.

1. Introduction

The Finite Elements Method (FEM) is very well suited to study the strain and stress distributions during heterogeneous deformation. The classical rolling process, i.e., symmetric rolling (SR), is characterized by the symmetry of the upper and lower rolls (the same roll diameters, angular velocities and friction coefficients between them and a processed material). SR is commonly used in the industrial practice. The asymmetric rolling (AR) is realized in most cases by applying different peripheral velocities of the upper and lower rolls. Alternatively, friction coefficients between rolls and a processed material can have different values; this approach was examined in detail in [1]. The peripheral velocity difference can result from a difference of diameters of two rolls and/or their angular velocities. In the present work two identical rolls with different angular velocities are considered.

AR has a potential importance for industrial applications, because it reduces the applied rolling pressure and torque and modifies microstructure; especially it can also lead to the grain refinement, as shown in [2]. Moreover, the appearing shear deformation produces a more homogeneous microstructure, modifies resulting textures (the example studies of texture variation was done in [2] and [3]) and offers a new possibility of tailoring selected mechanical properties, for example plastic anisotropy or residual stress (as shown in [4]). It can be mentioned that also cross-rolling offers some of the above material modifications (modification of texture and residual stress was examined in [5] and [6]).

2. Modelling of asymmetric rolling using FEM

SR and AR processes were studied in the present work using dynamic analysis procedure of ABAQUS/Explicit calculation environment (calculations were based on the examples presented in [7]). Geometrical parameters applied in the simulations correspond to the material and rolling device used

* AGH UNIVERSITY OF SCIENCE AND TECHNOLOGY, FACULTY OF PHYSICS AND APPLIED COMPUTER SCIENCE, AL. A. MICKIEWICZA 30, 30-059 KRAKÓW, POLAND
** LSPM-CNRS, UNIVERSITÉ PARIS 13, 99, AV. J.B. CLEMENT, 93 430 VILLETANEUSE, FRANCE

by the authors (located in LSPM laboratory, University Paris 13). It was assumed that the initial thickness of the rolled material (ferritic low carbon steel) was 2.5 mm and that it was deformed till 10, 20 and 30% rolling reduction. The rolls of 66 mm diameter were modelled as rigid ones, using the *RIGID SURFACE option. The angular velocity of the lower roll was constant and equal to 2.77 rad/s, while different velocities of the upper roll were considered: 2.77, 2.67, 2.52, 2.4 and 2.31 rad/s. Consequently, the following angular velocity ratios, A= ω_1/ω_2, were obtained: 1, 1.04, 1.1, 1.15 and 1.20.

The mechanical properties of ferrite steel were characterized by: Young modulus, E=210 GPa, Poisson's ratio, ν =0.3 and by the plasticity with isotropic hardening, without strain rate sensitivity. The simulations were performed assuming a constant friction coefficient, μ =0.3, the same at two rolls (it is a typical value in rolling process [8]). The contact between the rolls and the sample was modelled with the *CONTACT PAIR option. The rolling process was modelled using 4-node, bilinear, reduced integration and hourglass controlled procedure.

The frequent problem, especially important in sequential rolling, is the appearance of the inclined entry of a sheet – Fig. 1. The values between 0° and 6° of the entry angle, α, were considered in the calculations. The last value is a typical one, appearing in practical applications.

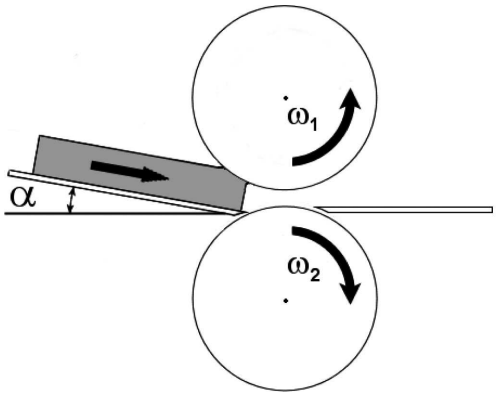

Fig. 1. Scheme of asymmetric rolling with inclined entry, used in calculations

In order to obtain stable solutions by ABAQUS/Explicit solver, the kinetic energy was controlled during calculations. In a quasi static process, the kinetic energy of the deformed material should not exceed a small fraction (typically 10%) of the internal energy [9]. The loading rates inferior than 1% of the wave speed u in the material were used in the calculations. The numerical stability restricts the time increment in the explicit approach to:

$$\Delta t \leqslant \frac{L}{u} \quad with \quad u = \sqrt{\frac{E}{\rho}} \tag{1}$$

where L is the characteristics length of an element, ρ is the density of the material and the minimum Δt is selected over all elements in the mesh. In other words, the time increment has to be shorter than a time required for wave propagation across the smallest element, hence usually it is very small.

The results obtained in our calculations were divided into two groups: external characteristics of the rolling process (applied forces, torques, bend magnitude, deformation work) and material characteristics (internal and residual stress, local strain, crystallographic texture). The first group is important for planning a deformation process, while the second one concerns properties of the processed material.

3. External characteristics of the rolling process

The calculated shape and strain distribution of the rolled plate after SR and AR are shown in Fig. 2. In agreement with experimental observations, the results of simulation confirmed that AR sample was bent. Bending is a typical behaviour of AR sheet and was analysed by different authors, e.g., [10,11]. Generally, bending of the rolled material is an undesirable effect. However, it can be advantageous in some cases, for example for bending a rolled sheet on the last mill in a sequential rolling, directly before a coiling operation. The calculated bend magnitude versus ω_1/ω_2 is shown in Fig. 3a. It is visible that bending can be controlled by an appropriate choice of ω_1/ω_2 for a given rolling reduction. On the other hand, as expected, no bending was predicted by FEM calculation for symmetric rolling: ω_1/ω_2 =1.

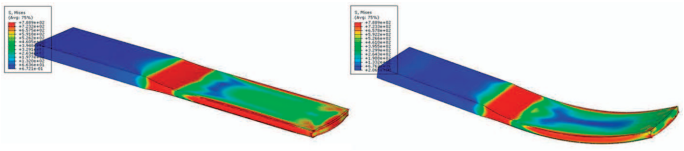

Fig. 2. Shape of the bar rolled to 30% reduction and its strain distribution – calculated by FEM for symmetric (ω_1/ω_2 = 1) and asymmetric rolling (ω_1/ω_2 = 1.1)

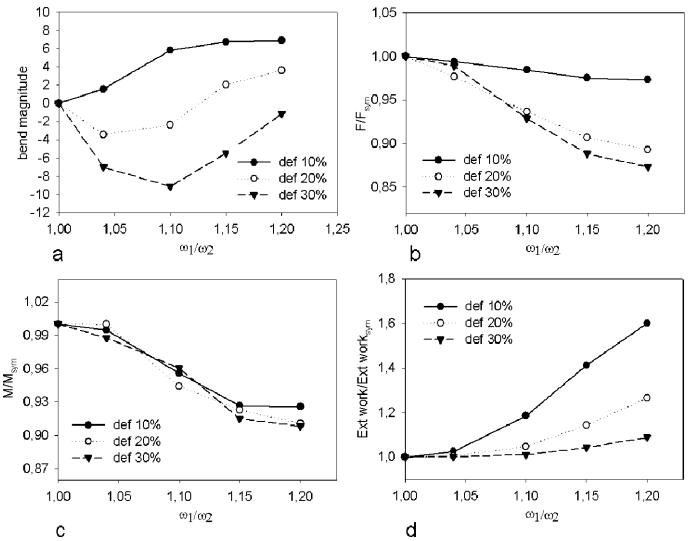

Fig. 3. Basic mechanical characteristics versus ω_1/ω_2 predicted by FEM for asymmetric rolling and for entry angle α =0°. Following results for 10%, 20%, 30% rolling reductions are presented: a) bend magnitude defined as the deflection (in mm) at the end of 200 mm rolled plate, b) relative normal force (F_{AR}/F_{SR}), c) relative torque (M_{AR}/M_{SR}), and d) relative deformation work (W_{AR}/W_{SR})

Other characteristics of AR, predicted by FEM calculations, are shown in Fig. 3 b,c and d. These results are presented in relative units, each quantity for AR is normalized with respect to SR (e.g., normal force is presented as F_{AR}/F_{SR}). We

note from Figs. 3 b, c that normal force and torque required for a given strain are lower in AR compared with SR. These two quantities decrease versus the degree of asymmetry (ω_1/ω_2). Moreover, the reduction of normal force depends strongly on deformation. The reduction of torque and normal force is of potential interest in aspect of the rolling mill durability. On the other hand, the external work (total deformation work) increases with the degree of rolling asymmetry (ω_1/ω_2), but this effect weakens with the progressing deformation (Fig. 3d).

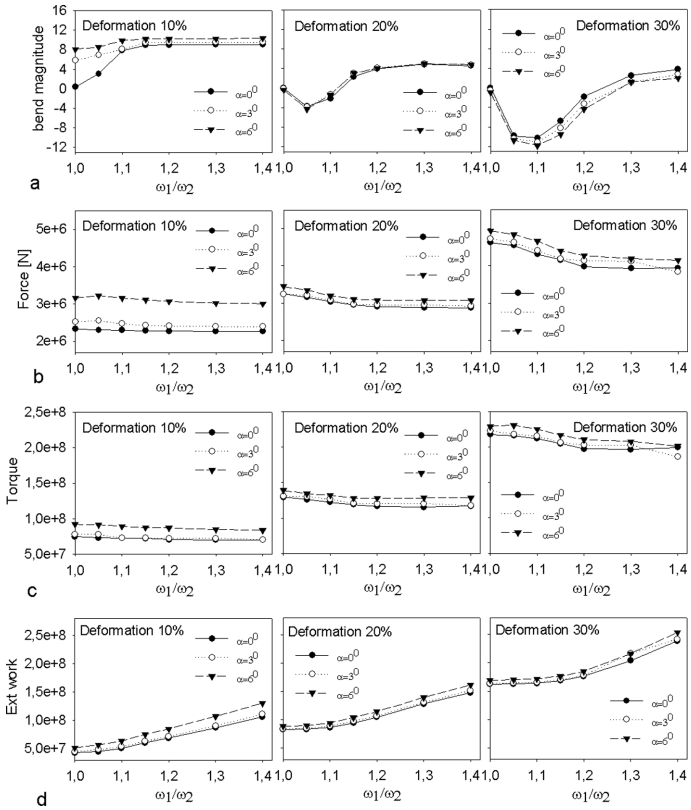

Fig. 4. Mechanical characteristics versus ω_1/ω_2 predicted by FEM for asymmetric rolling in the case of different entry angles α (0°, 3°, 6°). Results for 10%, 20%, 30% rolling reductions are presented: a) bend magnitude defined as the deflection (in mm) at the end of 200 mm rolled plate, b) normal force, c) torque, d) deformation work

The results presented in Fig. 3 were obtained assuming a flat entry of the sheet to the rolling mill (α =0° – see Fig. 1). However, in many cases, especially during sequential rolling, a sheet can enter to the next rolling mill obliquely (i.e., with α>0°). To study this effect, the bend magnitude, normal force, torque and external work were calculated for three entry angles: α =0^0, α =3°, α =6° and for three values of the final deformation: 10%, 20% and 30%. These results are presented vs. ω_1/ω_2 in Fig. 4. We note that all considered quantities (bend magnitude, normal force, applied torque and external work) have higher values for higher angle α. The dependence on α is the most marked in the case of 10% rolling reduction. Let us also note a strong dependence of the bend magnitude on the rolling asymmetry (ω_1/ω_2), especially for 20% and 30% deformations. Therefore, by a convenient choice of the rolling asymmetry and the entry angle, one can obtain a given amount of the bend magnitude.

4. Material characteristics

4.1. Internal and residual stress distributions

Selected results of the calculated stress distribution in the rolling gap (internal stresses) corresponding to the rolling reduction of 20% are collected in Fig. 5 (entry angle α =0°) and in Fig. 6 (entry angle α =6°).

Let us consider first the flat entry of a material (α =0°– Fig.5). Characteristic variation of the shear stress component in the RD-ND plane, i.e., Σ_{13} one, appears on both surfaces of AR sample. Let us consider the variation of internal stresses on the top surface of AR sample (Fig. 5a). For the angular velocity ratio, ω_1/ω_2, equal to 1, the sign of the shear component Σ_{13} is mainly positive. When the angular velocity ratio increases, the negative part of the shear component becomes smaller and for the velocity ratio of 1.15 the sign of this shear component is only positive. Similarly, in bottom surface layer, the Σ_{13} component tends to have increasingly positive value with growing angular velocity ratio, ω_1/ω_2 (Fig. 5c). In the central layer of the sample (Fig. 5b) the behaviour of this component is different in two types of rolling: in SR (i.e., for ω_1/ω_2 =1) the Σ_{13} component practically disappears during the whole rolling pass, while in AR a small variation of this component exists. The Σ_{13} stress component distribution is mainly responsible for sample bending and for crystallographic texture variation across the sample. The distributions of normal stress components (Σ_{33}, Σ_{11} and Σ_{22}) differ only slightly for two surface layers in AR mode. A different distribution of these components appears in the central layer. An interesting observation is a slight decrease of the normal stress component Σ_{33} in the central layer for ω_1/ω_2 = 1.15, compared with the cases of ω_1/ω_2 equal to 1.04 and 1 - Fig. 5b.

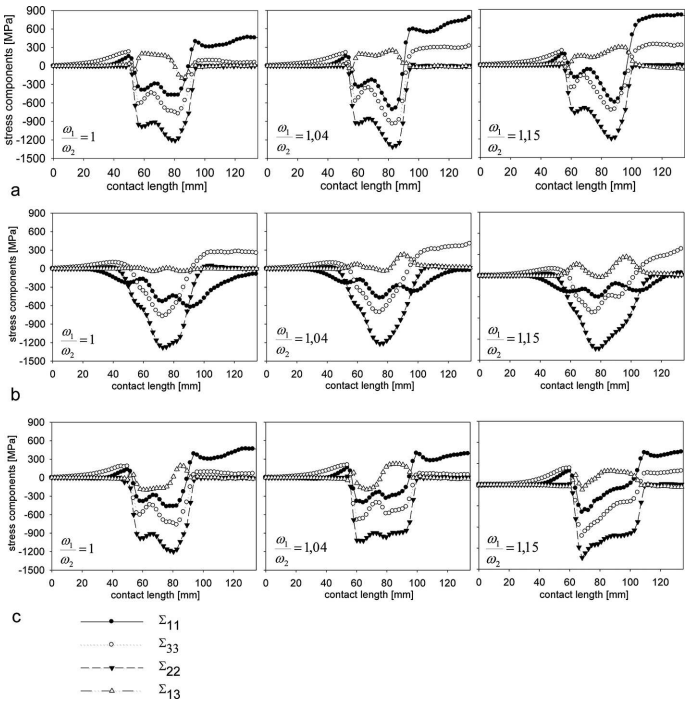

Fig. 5. Stress components for AR along the contact length: a) top surface, b) centre of the sample, c) bottom surface. Results for ω_1/ω_2 equal to 1, 1.04 and 1.15 are shown. Rolling reduction is 20% and entry angle α =0° (FEM calculation)

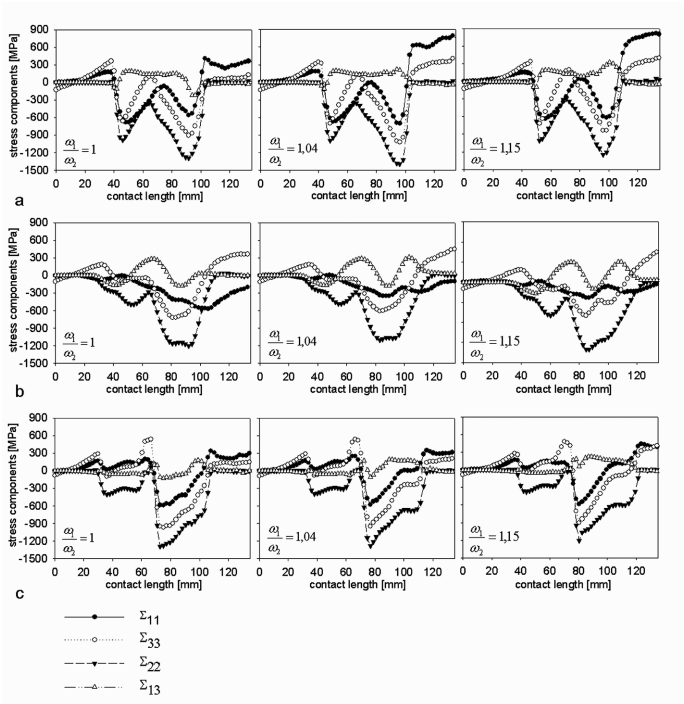

Fig. 6. Stress components for AR along the contact length: a) top surface, b) centre of the sample, c) bottom surface. Results for ω_1/ω_2 equal to 1, 1.04 and 1.15 are shown. Rolling reduction is 20% and entry angle α =6°(FEM calculation)

The internal stress distribution during an inclined entry (α =6°), is shown in Fig. 6. In this case the stress distribution in the rolling gap is more complex. In general, we observe much stronger oscillations of all stress components than in the case of the flat entry. A characteristic example is the oscillation of Σ_{33} component in three layers of the material. The described internal stress variations can strongly modify the material characteristics, e.g., crystallographic texture and material microstructure.

Another important material characteristics are the residual stresses (Σ_{ij}^{res}). They remain in a sample after plastic deformation and they are important for material properties, as discussed in [12-14]. FEM predictions of residual stress vs. distance from the sample surface for entry angle α =0° and for ω_1/ω_2 = 1, 1.05 and 1.15 – are shown in Fig. 7. The Σ_{33}^{res} and Σ_{13}^{res} components have relatively small magnitudes (they do not exceed 50 MPa). In contrast, the values and variations of Σ_{11}^{res} and Σ_{22}^{res}components are significantly higher (amplitudes of 800 MPa and 200 MPa, respectively). In general, residual stress components have different distributions after AR and SR processes. In the case of SR (ω_1/ω_2 =1), theΣ_{11}^{res}, $\Sigma_{22}^{res}$and Σ_{33}^{res} components have symmetrical distributions with respect to the sample centre, while Σ_{13}^{res} component shows a characteristic oscillating variation with a change of sign. In contrary, in the case of AR (ω_1/ω_2 = 1.15) all components have much less symmetric distributions. The most important differences of residual stress components between SR and AR processes appear on the top surface. Moreover, in the central sample volume the Σ_{33}^{res} component is lower after AR process (ω_1/ω_2 = 1.05 and 1.15) than after SR one, which can be associated with the reduction of the normal force during AR process (cf. Figs. 3b and 5b).

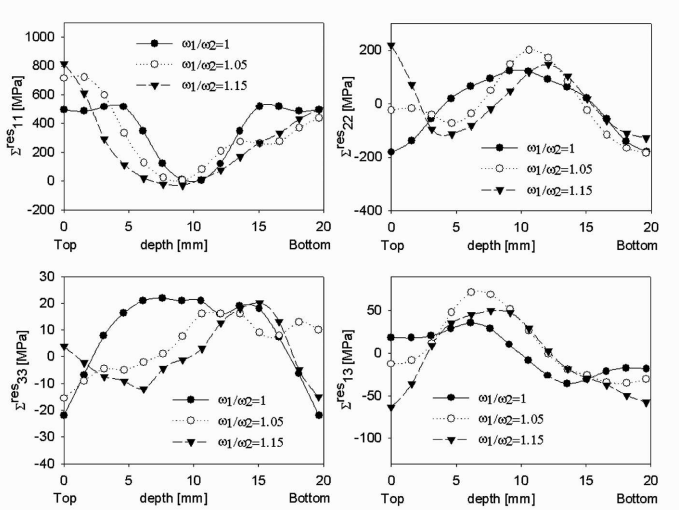

Fig. 7. Residual stress components (Σ_{11}^{res}, Σ_{22}^{res}, Σ_{33}^{res}, Σ_{13}^{res}) vs. distance from the sample surface (depth) for ω_1/ω_2 = 1, 1.05 and 1.15. The entry angle is α =0° (FEM calculation)

Finally, the variation of Von Mises equivalent residual stress versus depth is shown in Fig. 8 for ω_1/ω_2 = 1, 1.05, 1.15, for the rolling reductions of 10% and 30% and for two values of entry angle: α =0° and α =6°. It can be noted that for α =0^0 the distributions of equivalent residual stress are symmetrical with respect to the sample centre, while for α =6° this symmetry disappears. Moreover, in the case of AR (ω_1/ω_2 =1.05 and 1.15), the equivalent stress is higher in the top surface layer than in the bottom one, especially for 10% deformation and α =6°. Hence, we can conclude that the inclined entry modifies the residual stress state, especially on the sample surfaces. This has influence on material properties, like hardness, resistance for corrosion or recrystallization kinetics.

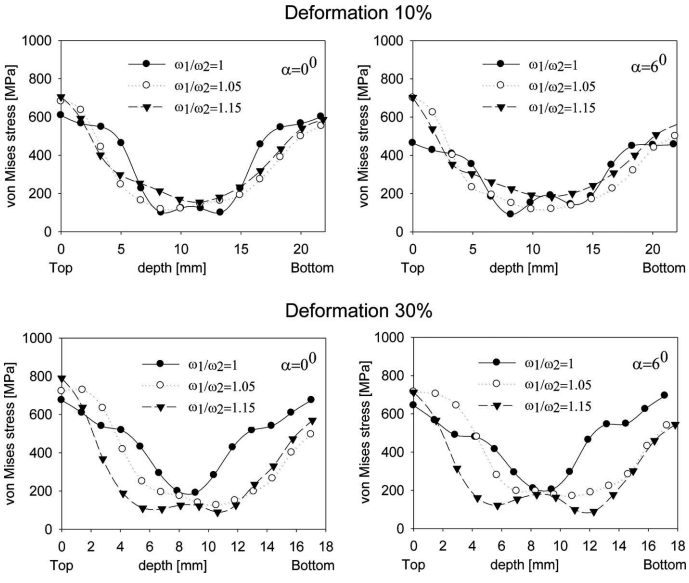

Fig. 8. Von Mises equivalent residual stress in function of depth for SR and AR processes. Results for rolling reductions of 10% and 30% and entry angles α =0° and α =6° are shown (FEM calculation)

4.2. Verification of calculated internal stress distribution – prediction of crystallographic textures

In order to verify the calculated internal stress distributions, they were used for the prediction of rolling textures of low carbon ferritic steel. The textures were calculated using stress distributions for the top surface and central sample layers. The internal stress distributions, Σ_{ij}, for symmetric (ω_1/ω_2 =1) and asymmetric rolling (ω_1/ω_2 =1.04), in the case of flat material entry (α =0), from Figs. 5a and b were applied in the crystallographic deformation model [15]. This model predicts texture and mechanical characteristics basing on crystallographic slip inside grains. The grain-matrix interaction is described by the relation:

$$\dot{\sigma_{ij}} = \dot{\Sigma}_{ij} + L(\dot{E}^p_{ij} - \dot{\varepsilon}^p_{ij}) \tag{2}$$

where σ_{ij} and ε^p_{ij} are stress and plastic strain tensors of a grain, Σ_{ij} and E^p_{ij} are analogous quantities for the sample and L is the scalar interaction parameter (L =1000 MPa was used for low carbon steel). Knowing a local grain stress state, σ_{ij}, the active slip systems are selected and grain strain and lattice rotation are calculated. This enables the calculation of crystallographic textures resulting from plastic deformation.

The predicted and experimental textures of the initial and rolled materials for the top and central sample layers are shown in Figs. 9-11. The orientation distribution functions (ODF) are presented, according to Bunge convention [16]. Experimental textures were determined by X-ray diffraction for the top and the central layers by mechanical removing of the material [17, 18]. It can be mentioned that it is also possible to examine the texture and stress heterogeneity in a non-destructive way [19-22].

The texture of the central layer practically did not change after rolling, both in symmetric and asymmetric modes (compare Figs. 9 and 10); it is a typical b.c.c. rolling texture. In contrary, we note a strong texture modification in the surface layer after rolling (compare Figs. 9 and 11): it changed from f.c.c. type rolling texture to a typical b.c.c. one. In the case of asymmetric rolling it is, moreover, rotated about 10 degs around the transverse direction compared with the symmetric case. All these textures were correctly predicted by the crystallographic deformation model – Figs. 10 and 11. We observe a good agreement between the measured and experimental textures, which confirms a correct prediction of internal stresses by FEM and a good construction of crystallographic deformation model.

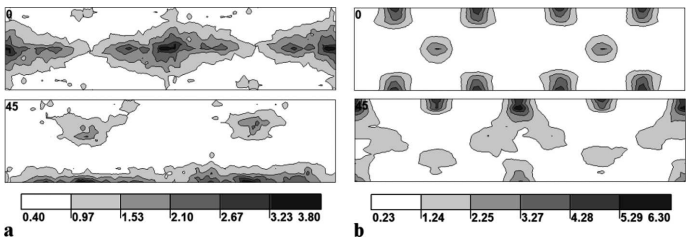

Fig. 9. Measured crystallographic texture of ferritic steel for the initial material: a) top surface of the sample, b) centre of the sample. Sections of the orientation distribution function (ODF) for ϕ_2 =0° and ϕ_2 =45° are shown

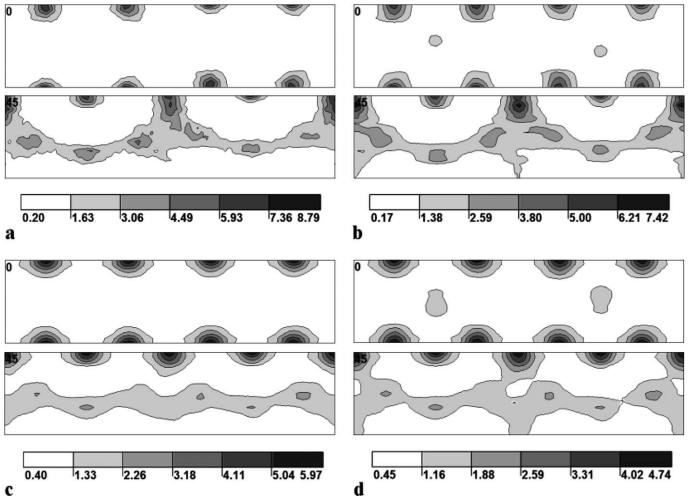

Fig. 10. Measured and predicted orientation distribution functions (ODFs) of the central layer of the sample (25% rolling reduction): a) experimental ODF after symmetric rolling (ω_1/ω_2 =1), b) experimental ODF after asymmetric rolling (ω_1/ω_2 =1.04), c) predicted ODF for symmetric rolling, d) predicted ODF for asymmetric rolling. Sections for ϕ_2 =0° and ϕ_2 =45° are shown

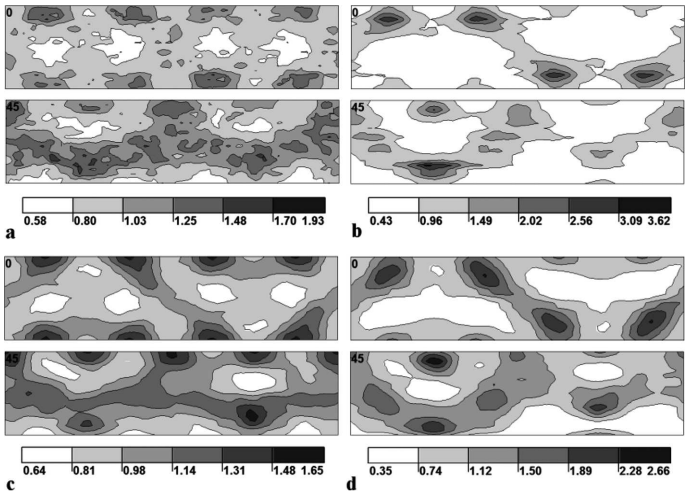

Fig. 11. Measured and predicted orientation distribution functions (ODFs) for the top layer of the sample (25% rolling reduction): a) experimental ODF after symmetric rolling (ω_1/ω_2 =1), b) experimental ODF after asymmetric rolling (ω_1/ω_2 =1.04), c) predicted ODF for symmetric rolling, d) predicted ODF for asymmetric rolling. Sections for ϕ_2 =0° and ϕ_2 =45° are shown

4.3. Local strain distributions

Distributions of the local strain were also calculated. FEM predictions of strain components $\varepsilon_{11}, \varepsilon_{22}, \varepsilon_{33}, \varepsilon_{13}$ versus depth for the entry angle α =0° and for ω_1/ω_2 = 1, 1.05, 1.15 are shown in Fig. 12. The strain components ε_{11} and ε_{33} have predominant values compared with ε_{22} and ε_{13} ones. In general, strain components have different distributions in AR and SR cases. In the case of SR (ω_1/ω_2 = 1), the ε_{11}, ε_{22} and ε_{22} components have symmetrical distributions with respect to the sample centre, while the ε_{13} component shows a typical oscillation with a change of sign.

Finally, the variation of equivalent plastic strain versus depth is shown in Fig.13 for ω_1/ω_2 equal to 1, 1.05 and 1.15,

for rolling reductions of 10% and 30% and for two values of entry angle α: 0° and 6°. It can be noted that for α =0° and for SR the distributions of equivalent strain are symmetrical with respect to the sample centre, while for α =6° they are significantly asymmetrical. The most important difference of strain components between SR and AR cases for α =0° appears on the top surface. It is interesting to note that in the case of 10% deformation and α =6° the strain distribution across the sample is more homogeneous after asymmetric rolling (ω_1/ω_2 =1.15) than after symmetric one. Moreover, an important feature can be observed: for both entry angles (α =0° and α =6°) and in the whole cross-section of the sample, the equivalent strain is distinctly higher for AR (ω_1/ω_2 =1.05 and 1.15) than for SR. Consequently, we can conclude that AR leads to higher local deformations, hence to a stronger material fragmentation.

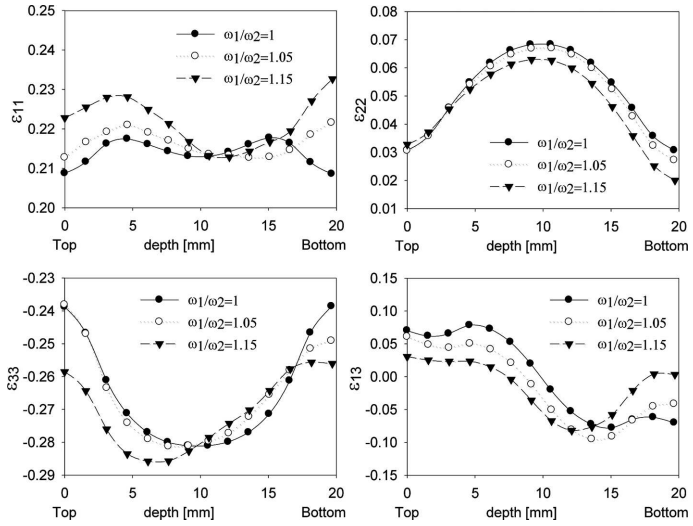

Fig. 12. Strain components $\varepsilon_{11}, \varepsilon_{22}, \varepsilon_{33}, \varepsilon_{13}$ vs. distance from the sample surface (depth) after SR and AR with ω_1/ω_2 = 1, 1.05 and 1.15. Entry angle α =0° (FEM calculation)

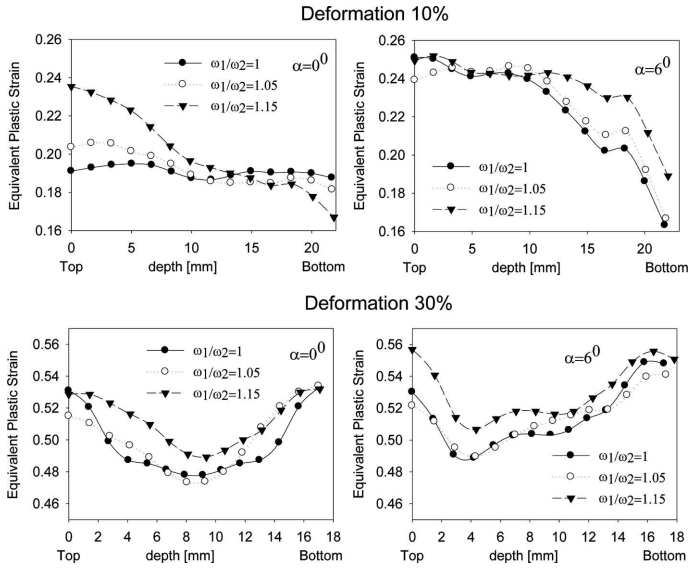

Fig. 13. Equivalent plastic strain vs. distance from the sample surface (depth) for SR and AR. Results for 10% and 30% rolling reductions and for entry angles α =0° and α =6° are shown (FEM calculation)

5. Conclusions

Our calculations lead to the following conclusions:

- Stress and strain distributions produced by symmetric and asymmetric rolling are different. In all the cases they depend on the velocity ratio (ω_1/ω_2) and on the entry angle (α). Modifications of stress and strain distribution introduced by asymmetric rolling can be used to change crystallographic textures and some mechanical properties of a material. In asymmetric rolling a higher local deformation is observed, which causes a stronger material fragmentation.
- Asymmetric rolling lowers the applied torque and normal rolling force, which is advantageous for rolls durability.
- After asymmetric rolling a bending of material appears, which is characterized by the bend magnitude. In most cases it is undesirable effect, but sometimes it may be advantageous. Bend magnitude depends on the velocity ratio (ω_1/ω_2), the final deformation and the entry angle of a plate. The bend magnitude can be reduced by an appropriate choice of these parameters, which can be optimized by FEM calculation before a real rolling process.
- Calculated distribution of internal stress was applied to predict the crystallographic textures of the rolled low carbon steel. They are in good agreement with experimental data.

Acknowledgements

The study was financed by the grants of the Polish National Centre for Science (NCN): DEC-2011/01/B/ST8/07394 and DEC-2011/01/D/ST8/07399. The support of the French ANR 05-BLAN-0383 project is also acknowledged.

REFERENCES

[1] H. Gao, S.C. Ramalingam, G.C. Barber, G. Chen, Analysis of asymmetrical cold rolling with varying coefficients of friction, J. Mater. Process. Technol. **124**, 178-182 (2002).

[2] H. Jin, D.J. Lloyd, Evolution of texture in AA6111 aluminum alloy after asymmetric rolling with various velocity ratios between top and bottom rolls. Mat. Sci. Eng. A. **465**, 267-273 (2007).

[3] S.H. Lee, D.N. Lee, Analysis of deformation textures of asymmetrically rolled steel sheets, Int. J. Mech. Sci. **43**, 1997-2015 (2001).

[4] S. Wronski, B. Ghilianu, T. Chauveau, B. Bacroix, Analysis of textures heterogeneity in cold and warm asymmetrically rolled aluminium, Mater. Character. **62**, 22-34 (2011).

[5] K. Wierzbanowski, S. Wronski, A. Baczmanski, M. Wróbel, C.Braham, M. Fitzpatrick, A. Lodini, Residual Stresses Induced by Cross-Rolling, Mat. Sci. Forum **524-525**, 63-68 (2006).

[6] S. Wronski, M. Wrobel, A. Baczmanski, K. Wierzbanowski, Effects of cross-rolling on residual stress, texture and plastic anisotropy in f.c.c. and b.c.c. metals, Mater. Character. **77**, 116-126 (2013).

[7] H.D. Hibbitt, B.I. Karlson, D. Sorensen, ABAQUS Example Problems Manual. Rolling of Thick Plates (1.3.6), pp. 485-502, 2004.

[8] M. Pietrzyk, J.G. Lenard, Thermal-Mechanical Modelling of the Flat Rolling Process, Springer, Berlin, Germany, 1991.

[9] H.D. Hibbitt, B.I. Karlson, D. Sorensen, ABAQUS Analysis User's Manual version 6.7, 2007.

[10] J.S. Lu, O.K. Harrer, W. Schwenzfeier, F.D. Fischer, Analysis of the bending of the rolling material in asymmetrical sheet rolling, Int. J. Mech. Sci. **42**, 49-61 (2000).

[11] S.A.A. Akbari Mousavi, S.M. Ebrahimi, R. Madoliat, Three dimensional numerical analyses of asymmetric rolling, J. Mater. Process. Technol. **187-188**, 725-729 (2007).

[12] A. Baczmanski, K. Wierzbanowski, C. Braham, A. Lodini, Internal Stresses in two Phase Polycrystalline Materials, Archives of Metallurgy **44**, 39-50 (1999).

[13] A. Baczmanski, P. Lipinski, A. Tidu, K. Wierzbanowski, B. Pathiraj, Quantitative estimation of incompatibility stresses and elastic energy stored in ferritic steel, J. Appl. Cryst. **41**, 854-867 (2008).

[14] K. Wierzbanowski, J. Tarasiuk, B. Bacroix, A. Miroux, O. Castelnau, Deformation Characteristics Important for Nucleation Process. Case of Low-Carbon Steels, Archives of Metallurgy **44**, 183-201 (1999).

[15] K. Wierzbanowski, A. Baczmanski, P. Lipinski, A. Lodini, Elasto-plastic models of polycrystalline material deformation and their applications, Arch. Metall. Mater. **52**, 77-86 (2007).

[16] H.J. Bunge, Texture Analysis in Materials Science, Butterworths, London, 1982.

[17] S. Wronski, K. Wierzbanowski, B. Bacroix, M. Wróbel, E. Rauch, F. Montheillet, M. Wronski, Texture heterogeneity of asymmetrically rolled low carbon steel, Arch. Metall. Mater. **54**, 89-102 (2009).

[18] S. Wronski, K. Wierzbanowski, B. Bacroix, M. Wróbel, T. Chauveau, M. Wronski, Crystallographic Textures Variation in Asymmetrically Rolled Steel, Mater. Sci. Forum **638-642**, 2811-2816 (2010).

[19] J. Tarasiuk, K. Wierzbanowski, A. Baczmanski, Application of the Method for Non-Destructive Evaluation of Texture Heterogeneity, Mater. Sci. Forum **157-162**, 213-220 (1994).

[20] J. Tarasiuk, K. Wierzbanowski, A. Baczmanski, New Algorithm of Direct Method of Texture Analysis, Cryst. Res. Technol. **33**, 101-118 (1998).

[21] S. Wroński, K. Wierzbanowski, A. Baczmański, A. Lodini, Ch. Braham, W. Seiler, X-ray grazing incidence technique – corrections in residual stress measurement – A review, Powder Diffraction Suppl. **24**, S1-S15 (2009).

[22] A. Baczmański, K. Wierzbanowski, J. Tarasiuk, M. Ceretti, A. Lodini, Anisotropy of Micro-Stresses Measured by Diffraction, Revue de Metallurgie **94**, 1467-1474 (1997).

Received: 10 March 2014.